IEEE Open Journal of Vehicular Technology

Received 14 November 2023; accepted 22 November 2023. Date of publication 27 November 2023;
date of current version 18 December 2023. The review of this article was coordinated by Editor Edward Kwok Shum Au.

Digital Object Identifier 10.1109/OJVT.2023.3336619

Capacity Analysis of UAV-to-Ground Channels With Shadowing: Power Adaptation Schemes and Effective Capacity

REMON POLUS (Graduate Student Member, IEEE), AND CLAUDE D'AMOURS (Member, IEEE)

School of Electrical Engineering and Computer Science, University of Ottawa, Ottawa, ON K1N 6N5, Canada

CORRESPONDING AUTHOR: REMON POLUS (e-mail: rpolus@uottawa.ca)

This work was supported in part by the C. D'Amours' Natural Sciences and Engineering Research Council of Canada (NSERC) Discovery under Grant RPGIN 2022-03421.

ABSTRACT In this article, an unmanned aerial vehicle (UAV), acting as a transmitter, employs different power adaptation strategies in order to enhance the ergodic capacity of the wireless channel between it and a receiver on the ground. We present the derivation of closed-form expressions for the channel capacity of the recently developed UAV-to-ground fading channels under different power adaptation strategies. The power adaptation strategies considered in this paper are optimal rate adaptation with fixed power (ORA), optimal power and rate adaptation (OPRA), channel inversion with fixed rate (CIFR), and truncated channel inversion with fixed rate (TIFR). In addition to ergodic capacity analysis, precise analytical formulas for the effective capacity of the UAV-to-ground fading channels are derived. Additionally, all of these closed-form expressions are verified by comparing them with numerical results obtained through Monte Carlo simulations.

INDEX TERMS Unmanned aerial vehicles (UAVs), power adaptation, effective capacity.

I. INTRODUCTION

Recently, unmanned aerial vehicles (UAVs) have become a promising candidate technology for beyond fifth-generation (5G) systems due to their high mobility and reasonable deployment costs [1], [2], [3]. Moreover, a UAV can be deployed in various scenarios related to wireless communications and networking such as acting as an aerial base station, an aerial relay node, or as the wireless backhaul of the network [4], [5], [6]. This has motivated many researchers to develop fading channel models that can best describe the received signal's fluctuation in the communication link between a UAV in the air and a receiver (Rx) on the ground [7], and [8]. These new models were developed based on Nakagami-*m* and inverse-gamma distributions to model multipath and shadowing effects respectively.

Recently, scholars have investigated the performance of wireless communication systems operating over UAV-to-ground channels. The average bit error rate (ABER), average ergodic channel capacity, and outage probability for the UAV-to-ground channels were all examined by the authors of [7]. Additionally, the authors of [9] only included the average symbol error rate (ASER) for quadrature amplitude modulation (QAM) schemes in their research. Maximum ratio combining (MRC) performance was the focus of [10]. However, these previous papers considered the constant transmit power case, referred to as optimal rate adaptation (ORA), and did not investigate the effect of power adaptation methods to improve the ergodic capacity of the channel.

In this paper, we consider other power adaptation techniques in addition to ORA. In optimal power and rate adaptation (OPRA), the channel fade level is tracked by both the transmitter (Tx) and Rx, while in ORA, it is tracked by the Rx alone. Thus, the OPRA requires feedback between the Rx and Tx, which results in a higher complexity compared to ORA. Two suboptimal adaptive techniques are considered, which are channel inversion with fixed rate (CIFR), and truncated channel inversion with fixed rate (TIFR). In previous research work, the channel capacity was studied under different power adaptation schemes over various fading channels (e.g., Rayleigh [11], [12], Nakagami-*m* [13], Fluctuating Two-Ray [14], and Fisher-Snedecor $\mathcal{F}$ [15]).

Shannon's ergodic capacity has widely been used, but it is not able to measure the system performance under quality of service (QoS) constraints such as system delay and data rate. Effective capacity has been proposed as an alternative

performance metric owing to its ability to take into account the system's delay constraint [16]. Additionally, computation of the effective capacity offers an efficient and convenient way to evaluate the statistical QoS performance of wireless systems from the networking perspective. This includes the analysis of resource allocation management, spectral efficiency, user scheduling schemes, and cognitive radio networks [17].

To the best of our knowledge, the effective capacity and ergodic capacity of UAV communications under different power adaptation schemes over shadowed fading channels have not been investigated in the literature. This paper is the first to evaluate the average ergodic channel capacity for each scheme under the novel UAV-to-ground channel models with shadowing, yielding closed-form expressions. Moreover, the effective capacity of these channels is studied. The contributions of this paper are as follows.

- Closed-forms expressions of the signal-to-noise ratio (SNR) moments are derived in order to evaluate the amount of fading of the UAV-to-ground fading channels.
- For each of the ORA, OPRA, CIFR, and TIFR adaptive transmission protocols, closed-forms expressions of the average channel capacity are obtained.
- Obtaining analytical expressions for the effective capacity of UAV-to-ground fading channels.
- These closed-form expressions perfectly match with the numerical results obtained by Monte Carlo simulation, which in turn validates the accuracy of the theoretical analysis provided in this paper.

This paper is organized as follows. In Section II, a mathematical overview of the UAV-to-ground channel models is provided. In Sections III and IV, the amount of fading and capacity analysis for different power adaptation methods are derived respectively. Section V focuses on the effective capacity analysis. Finally, numerical results and conclusions are discussed in Sections VI and VII, respectively.

The following mathematical notations are used throughout this paper. $\mathbb{E}(.)$, $\mathbb{P}(.)$, $f_X(.)$, and $F_X(.)$ represent the expectation, probability, probability density function (PDF), and cumulative distribution function (CDF) of a random variable X, respectively.

II. UAV CHANNEL MODELS

This section summarizes the UAV channel model under double-shadowing and single-shadowing communication scenarios.

A. DOUBLE-SHADOWING (DS) COMMUNICATION SCENARIO

In this scenario, a UAV in the air acts as a Tx and transmits a signal to a Rx node on the ground. Shadowing regions exist around both the Tx and Rx, which are separated by a large distance. The received SNR, γ, can be modeled as

$$\gamma = N_1^2 I_1 N_2^2 I_2, \tag{1}$$

where

- $N_j - j \in \{1, 2\}-$ represents the multipath fading coefficient which follows the Nakagami-m distribution [18]. The PDF of N_j^2 can be written as

$$f_{N_j^2}(x) = \frac{{m_j}^{m_j} x^{m_j - 1}}{{\Omega_j}^{m_j} \Gamma\left(m_j\right)} e^{-\frac{m_j x}{\Omega_j}}, \qquad x > 0, \tag{2}$$

  where the distribution's shaping parameter m_j is the fading severity parameter, Ω_j is the scale parameter, and $\Gamma(.)$ is the gamma function.
- I_j represents the shadowing effect of the channel, modeled by the inverse gamma (IG) distribution [19], whose PDF can be written as

$$f_{I_j}(x) = \frac{{\overline{\gamma}_j}^{\alpha_j}}{x^{\alpha_j + 1} \Gamma\left(\alpha_j\right)} e^{-\frac{\overline{\gamma}_j}{x}}, \qquad x > 0, \tag{3}$$

  where the shaping parameter of the distribution $\alpha_j > 1$ represents the severity of the shadowing and $\overline{\gamma}_j$ denotes the scaling parameter.

The PDF of the received SNR can be given by [7]

$$\begin{aligned} f_\gamma(\gamma) &= \frac{\mathbb{S}_{DS}}{\gamma} G_{2,2}^{2,2}\left(\frac{m_1 m_2}{\overline{\gamma}}\gamma \middle| \begin{matrix} 1-\alpha_2, 1-\alpha_1 \\ m_1, m_2 \end{matrix}\right), \\ &= \frac{m_1 m_2}{\overline{\gamma}} \mathbb{S}_{DS} G_{2,2}^{2,2}\left(\frac{m_1 m_2}{\overline{\gamma}}\gamma \middle| \begin{matrix} -\alpha_2, -\alpha_1 \\ m_1 - 1, m_2 - 1 \end{matrix}\right), \end{aligned} \tag{4}$$

where $\mathbb{S}_{DS} = \frac{1}{\Gamma(m_1)\Gamma(m_2)\Gamma(\alpha_1)\Gamma(\alpha_2)}$, and $G_{p,q}^{m,n}(.|.)$ is the Meijer G-function [[20], eq. (9.301)], which is a built-in function in MATLAB. With the help of [21], (4) can be converted to an expression employing the Fox H-function as

$$\begin{aligned} f_\gamma(\gamma) = &\frac{m_1 m_2}{\overline{\gamma}} \mathbb{S}_{DS} \\ &\times H_{2,2}^{2,2}\left(\frac{m_1 m_2}{\overline{\gamma}}\gamma \middle| \begin{matrix} (-\alpha_2, 1), (-\alpha_1, 1) \\ (m_1 - 1, 1), (m_2 - 1, 1) \end{matrix}\right). \end{aligned} \tag{5}$$

The CDF of γ can be expressed as:

$$\begin{aligned} F_{\gamma(\gamma)} &= \int_0^\gamma f_\gamma(\prime\gamma) d\prime\gamma. \\ &= \mathbb{S}_{DS} G_{3,3}^{2,3}\left(\frac{m_1 m_2}{\overline{\gamma}}\gamma \middle| \begin{matrix} 1-\alpha_2, 1-\alpha_1, 1 \\ m_1, m_2, 0 \end{matrix}\right). \end{aligned} \tag{6}$$

B. SINGLE-SHADOWING (SS) COMMUNICATION SCENARIO

In the event of a single shadowing region located near one of the Tx or the Rx, the channel is categorized as a single-shadowing (SS) channel whose received SNR can be modeled as:

$$\gamma = N_1^2 N_2^2 I. \tag{7}$$

As shown in [7], the PDF of the received SNR can be represented as:

$$\begin{aligned} f_\gamma(\gamma) &= \frac{\mathbb{S}_{SS}}{\gamma} G_{1,2}^{2,1}\left(\frac{m_1 m_2}{\overline{\gamma}}\gamma \middle| \begin{matrix} 1-\alpha \\ m_1, m_2 \end{matrix}\right), \\ &= \frac{m_1 m_2}{\overline{\gamma}} \mathbb{S}_{SS}\, G_{1,2}^{2,1}\left(\frac{m_1 m_2}{\overline{\gamma}}\gamma \middle| \begin{matrix} -\alpha \\ m_1 - 1, m_2 - 1 \end{matrix}\right), \end{aligned} \tag{8}$$

where $\mathbb{S}_{SS} = \frac{1}{\Gamma(m_1)\Gamma(m_2)\Gamma(\alpha)}$. From [21], (8) can be expressed in terms of the Fox H-function as

$$f_\gamma(\gamma) = \frac{m_1 m_2}{\overline{\gamma}} \mathbb{S}_{SS} \times H_{1,2}^{2,1}\left(\frac{m_1 m_2}{\overline{\gamma}}\gamma \middle| \begin{matrix}(-\alpha, 1)\\ (m_1 - 1, 1), (m_2 - 1, 1)\end{matrix}\right). \quad (9)$$

The CDF of γ is:

$$F_\gamma(\gamma) = \mathbb{S}_{SS} G_{2,3}^{2,2}\left(\frac{m_1 m_2}{\overline{\gamma}}\gamma \middle| \begin{matrix}1-\alpha, 1\\ m_1, m_2, 0\end{matrix}\right). \quad (10)$$

III. AMOUNT OF FADING

According to [22], the amount of fading is a measure of the severity of the channel by itself, which can be calculated as

$$\mathcal{AF} = \frac{\mathbb{E}(\gamma^2)}{(\mathbb{E}(\gamma))^2} - 1, \quad (11)$$

where

$$\mathbb{E}(\gamma^n) = \int_0^\infty \gamma^n f_\gamma(\gamma) d\gamma, \quad (12)$$

where $n \in [1, 2]$.

1) *DS case:*
By substituting (5) in (12) and using [23], $\mathbb{E}(\gamma^2)$ and $\mathbb{E}(\gamma)$ can be evaluated for the DS case as shown in (13) and (14) respectively.

$$\mathbb{E}(\gamma^2) = \mathbb{S}_{DS}\left(\frac{m_1 m_2}{\overline{\gamma}}\right)^{-2} \Gamma(m_1+2)\Gamma(m_2+2) \times \Gamma(\alpha_1-2)\Gamma(\alpha_2-2). \quad (13)$$

$$\mathbb{E}(\gamma) = \mathbb{S}_{DS}\left(\frac{m_1 m_2}{\overline{\gamma}}\right)^{-1} \Gamma(m_1+1)\Gamma(m_2+1) \times \Gamma(\alpha_1-1)\Gamma(\alpha_2-1). \quad (14)$$

By substituting (13) and (14) into (11), we can obtain the amount of fading final expression as shown in (15), shown at the bottom of this page.

2) *SS case:*
Similarly for the SS case, $\mathbb{E}(\gamma^2)$ and $\mathbb{E}(\gamma)$ can be evaluated as shown in (16) and (17) respectively.

$$\mathbb{E}(\gamma^2) = \mathbb{S}_{SS}\left(\frac{m_1 m_2}{\overline{\gamma}}\right)^{-2} \Gamma(m_1+2)\Gamma(m_2+2) \times \Gamma(\alpha-2). \quad (16)$$

$$\mathbb{E}(\gamma) = \mathbb{S}_{SS}\left(\frac{m_1 m_2}{\overline{\gamma}}\right)^{-1} \Gamma(m_1+1)\Gamma(m_2+1) \times \Gamma(\alpha-1). \quad (17)$$

By plugging (16) and (17) into (11), we can derive the resulting expression for the amount of fading, as demonstrated in (18).

$$\mathcal{AF}_{SS} = \frac{\Gamma(m_1+2)\Gamma(m_2+2)\Gamma(\alpha-2)}{\mathbb{S}_{SS}[\Gamma(m_1+1)\Gamma(m_2+1)\Gamma(\alpha-1)]^2} - 1. \quad (18)$$

IV. ERGODIC CAPACITY ANALYSIS

A. OPTIMAL RATE ADAPTATION (ORA)

In this scheme, the Tx does not adjust its transmit power and just employs a constant power to transmit a signal to the destination. The ergodic capacity can be evaluated as

$$C_{\text{ORA}} = \frac{\mathbb{B}}{\ln(2)} \int_0^\infty \ln(1+\gamma) f_\gamma(\gamma) d\gamma, \quad (19)$$

where $\mathbb{B}$ is the channel bandwidth. To calculate the integral in (19), the natural logarithm function can be re-written as

$$\ln(1+\gamma) = G_{2,2}^{1,2}\left(\gamma \middle| \begin{matrix}1, 1\\ 1, 0\end{matrix}\right). \quad (20)$$

1) *DS case:*
By substituting (4) in (19), the integration in (19) involves the multiplication of two Meijer G-functions, which can be expressed, with the help of [24], in a closed-form expression as

$$C_{\text{ORA}} = \frac{\mathbb{B}\mathbb{S}_{DS}}{\ln(2)} G_{4,4}^{4,3}\left(\frac{m_1 m_2}{\overline{\gamma}} \middle| \begin{matrix}1-\alpha_2, 1-\alpha_1, 0, 1\\ m_1, m_2, 0, 0\end{matrix}\right). \quad (21)$$

2) *SS case:*
Similarly, if (8) is plugged into (19) for the SS case, C_{ORA} can be evaluated as

$$C_{\text{ORA}} = \frac{\mathbb{B}\mathbb{S}_{SS}}{\ln(2)} G_{3,4}^{4,2}\left(\frac{m_1 m_2}{\overline{\gamma}} \middle| \begin{matrix}1-\alpha, 0, 1\\ m_1, m_2, 0, 0\end{matrix}\right). \quad (22)$$

B. OPTIMAL POWER AND RATE ADAPTATION (OPRA)

In this power adaptation technique, the Tx adapts its transmit power, $P_t(\gamma)$, according to the instantaneous SNR value [11]. The relation between the transmit power and instantaneous SNR value can be written as

$$P_t(\gamma) = \overline{P} \max\left(\left(\frac{1}{\gamma_o} - \frac{1}{\gamma}\right), 0\right), \quad (23)$$

where $\overline{P}$ is the average power and γ_o is the optimal threshold SNR level below which no signal is transmitted, whose value is determined by [11]

$$\int_{\gamma_o}^\infty \left(\frac{1}{\gamma_o} - \frac{1}{\gamma}\right) f_\gamma(\gamma) d\gamma = 1. \quad (24)$$

The channel capacity under this scheme can be evaluated as

$$C_{\text{OPRA}} = \frac{\mathbb{B}}{\ln(2)} \int_{\gamma_o}^\infty \ln\left(\frac{\gamma}{\gamma_o}\right) f_\gamma(\gamma) d\gamma, \quad (25)$$

$$\mathcal{AF}_{DS} = \frac{\Gamma(m_1+2)\Gamma(m_2+2)\Gamma(\alpha_1-2)\Gamma(\alpha_2-2)}{\mathbb{S}_{DS}[\Gamma(m_1+1)\Gamma(m_2+1)\Gamma(\alpha_1-1)\Gamma(\alpha_2-1)]^2} - 1 \quad (15)$$

1) *DS case:*
Using the Fox H-function representation in (5) and following a similar approach to what is found in [25], C_{OPRA} can be evaluated, after some mathematical manipulations, for the DS case as

$$C_{\text{OPRA}} = \frac{\mathbb{B}\mathbb{S}_{DS}}{\ln(2)} \times G_{4,4}^{4,2}\left(\frac{m_1 m_2}{\overline{\gamma}}\gamma_o \middle| \begin{matrix} 1-\alpha_1, 1-\alpha_2, 1, 1 \\ 0, 0, m_1, m_2 \end{matrix}\right), \tag{26}$$

where the condition for γ_o is

$$\frac{m_1 m_2}{\overline{\gamma}}\mathbb{S}_{DS} G_{3,3}^{3,2}\left(\frac{m_1 m_2}{\overline{\gamma}}\gamma_o \middle| \begin{matrix} -\alpha_1, -\alpha_2, 1 \\ -1, m_1-1, m_2-1 \end{matrix}\right) = 1, \tag{27}$$

which can be evaluated numerically.

2) *SS case:*
Utilizing the Fox H-function representation in (9) and applying a comparable method to the analysis found in [25], C_{OPRA} for the SS case can be evaluated as

$$C_{\text{OPRA}} = \frac{\mathbb{B}\mathbb{S}_{SS}}{\ln(2)} G_{3,4}^{4,1}\left(\frac{m_1 m_2}{\overline{\gamma}}\gamma_o \middle| \begin{matrix} 1-\alpha, 1, 1 \\ 0, 0, m_1, m_2 \end{matrix}\right), \tag{28}$$

where the condition for γ_o is

$$\frac{m_1 m_2}{\overline{\gamma}}\mathbb{S}_{SS} G_{2,3}^{3,1}\left(\frac{m_1 m_2}{\overline{\gamma}}\gamma_o \middle| \begin{matrix} -\alpha, 1 \\ -1, m_1-1, m_2-1 \end{matrix}\right) = 1. \tag{29}$$

C. CHANNEL INVERSION WITH FIXED RATE (CIFR)

In this case, the Tx adjusts its transmit power in order to maintain a constant SNR at the Rx. This can be achieved by inverting the instantaneous channel state. The average channel capacity under this scheme can be evaluated as

$$C_{\text{CIFR}} = \mathbb{B}\log_2\left(1 + \frac{1}{\int_0^\infty \gamma^{-1} f_\gamma(\gamma)\, d\gamma}\right). \tag{30}$$

1) *DS case:*
By substituting (4) in (30) and using [23], the integration in (30) can be evaluated for the DS case as

$$\int_0^\infty \gamma^{-1} f_\gamma(\gamma)\, d\gamma = \mathbb{S}_{DS}\frac{m_1 m_2}{\overline{\gamma}}\Gamma(m_1-1)\Gamma(m_2-1) \times \Gamma(\alpha_1+1)\Gamma(\alpha_2+1). \tag{31}$$

2) *SS case:*
Likewise, in the case of SS, the integration in (30) can be assessed as follows:

$$\int_0^\infty \gamma^{-1} f_\gamma(\gamma)\, d\gamma = \mathbb{S}_{SS}\frac{m_1 m_2}{\bar{\gamma}}\Gamma(m_1-1) \times \Gamma(m_2-1)\Gamma(\alpha+1). \tag{32}$$

D. TRUNCATED CHANNEL INVERSION WITH FIXED RATE (TIFR)

When the transmission experiences a deep fade, a large amount of power is required to invert the channel gain. To avoid this, the channel inversion is only performed above a fixed cut-off value γ_o. If $\gamma < \gamma_o$, the channel is not used. The average channel capacity under this truncated channel inversion can be evaluated as [11]

$$C_{\text{TIFR}} = \mathbb{B}\log_2\left(1 + \frac{1}{\int_{\gamma_o}^\infty \gamma^{-1} f_\gamma(\gamma)\, d\gamma}\right)\mathbb{P}(\gamma > \gamma_o), \tag{33}$$

where γ_o is selected either to maximize C_{TIFR} or to achieve a specified outage probability.

1) *DS case:*
Utilizing the Fox H-function representation as described in (5), and adopting a methodology akin to the one presented in the work of [25], the integration in (33) for the DS case can be evaluated as

$$\int_{\gamma_o}^\infty \frac{f_\gamma(\gamma)}{\gamma} d\gamma = \mathbb{S}_{DS}\frac{m_1 m_2}{\overline{\gamma}} \times G_{3,3}^{2,3}\left(\frac{m_1 m_2}{\overline{\gamma}}\gamma_o \middle| \begin{matrix} -\alpha_2, -\alpha_1, 1 \\ 0, m_1-1, m_2-1 \end{matrix}\right). \tag{34}$$

$\mathbb{P}(\gamma > \gamma_o)$ can be computed as

$$\mathbb{P}(\gamma > \gamma_o) = 1 - \mathbb{S}_{DS} G_{3,3}^{2,3}\left(\frac{m_1 m_2}{\overline{\gamma}}\gamma_o \middle| \begin{matrix} 1-\alpha_2, 1-\alpha_1, 1 \\ m_1, m_2, 0 \end{matrix}\right). \tag{35}$$

2) *SS case:*
In a similar manner, the integration in (33) can be computed as

$$\int_{\gamma_o}^\infty \frac{f_\gamma(\gamma)}{\gamma} d\gamma = \mathbb{S}_{SS}\frac{m_1 m_2}{\overline{\gamma}} \times G_{2,3}^{3,1}\left(\frac{m_1 m_2}{\overline{\gamma}}\gamma_o \middle| \begin{matrix} -\alpha, 1 \\ 0, m_1-1, m_2-1 \end{matrix}\right). \tag{36}$$

The calculation of $\mathbb{P}(\gamma > \gamma_o)$ is achievable as

$$\mathbb{P}(\gamma > \gamma_o) = 1 - \mathbb{S}_{SS} G_{2,3}^{2,2}\left(\frac{m_1 m_2}{\overline{\gamma}}\gamma_o \middle| \begin{matrix} 1-\alpha, 1 \\ m_1, m_2, 0 \end{matrix}\right). \tag{37}$$

V. EFFECTIVE CAPACITY

As seen in [17], the effective capacity can be obtained by

$$C_{\text{E}} = \frac{-\mathbb{B}}{A}\log_2\left(\mathbb{E}\left[(1+\gamma)^{-A}\right]\right), \tag{38}$$

where

$$\mathbb{E}\left[(1+\gamma)^{-A}\right] = \int_0^\infty (1+\gamma)^{-A} f_\gamma(\gamma) d\gamma. \tag{39}$$

The term $(1+\gamma)^{-A}$ can be expressed in terms of Meijer G-function as

$$(1+\gamma)^{-A} = \frac{1}{\Gamma(A)} G_{1,1}^{1,1}\left(\gamma \middle| \begin{matrix} 1-A \\ 0 \end{matrix}\right). \tag{40}$$

The parameter A is evaluated as

$$A = \frac{\theta T \mathbb{B}}{\ln(2)}, \tag{41}$$

where θ is the buffer occupancy decay rate and T is the block length. we can observe that the effective capacity aligns with Shannon's classic ergodic capacity when there is no delay constraint as θ approaches zero.

1) *DS case:*
By substituting (4) and (40) in (39), the integration in (39) involves the multiplication of two Meijer G-functions, which can be expressed, with the help of [23], in a closed-form expression as

$$\int_0^\infty (1+\gamma)^{-A} f_\gamma(\gamma) d\gamma = \frac{\mathbb{S}_{DS}}{\Gamma(A)} \times G_{3,3}^{3,3}\left(\frac{m_1 m_2}{\overline{\gamma}} \middle| \begin{matrix} 1-\alpha_2, 1-\alpha_1, 1 \\ m_1, m_2, A \end{matrix}\right). \tag{42}$$

Thus, the final expression of the effective capacity for the DS case can be expressed as shown in (43), shown at the bottom of this page.

2) *SS case:*
Similarly for the SS case, the integration in (39) can be evaluated as

$$\int_0^\infty (1+\gamma)^{-A} f_\gamma(\gamma) d\gamma = \frac{\mathbb{S}_{SS}}{\Gamma(A)} \times G_{2,3}^{3,2}\left(\frac{m_1 m_2}{\overline{\gamma}} \middle| \begin{matrix} 1-\alpha, 1 \\ m_1, m_2, A \end{matrix}\right). \tag{44}$$

Thus, the closed-form expression of the effective capacity for the SS case can be formulated as shown in (45).

$$C_{\mathrm{E}}^{\mathrm{SS}} = \frac{-\mathbb{B}}{A} \log_2\left(\frac{\mathbb{S}_{SS}}{\Gamma(A)} G_{2,3}^{3,2}\left(\frac{m_1 m_2}{\overline{\gamma}} \middle| \begin{matrix} 1-\alpha, 1 \\ m_1, m_2, A \end{matrix}\right)\right). \tag{45}$$

VI. NUMERICAL RESULTS

In this section, we present some plots that illustrate the performance of UAV-to-ground channels with shadowing. For the Monte Carlo simulation, 10^6 realizations of fading channels are generated to validate the analytical expressions in the previous sections.

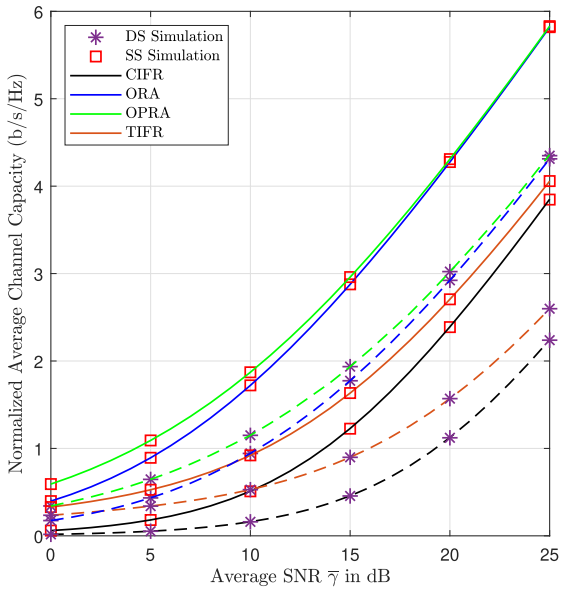

FIGURE 1. Normalized average channel capacity under different power adaptation schemes. Solid and dash lines represent corresponding analytical expressions of the SS case and DS one respectively.

TABLE 1 Simulation Parameters for Fig. 1

Parameter	m_1	m_2	α_1	α_2
Value	1.5	1.8	3.5	3.6

In Fig. 1, the normalized average channel capacity, $C/\mathbb{B}$, is plotted as a function of the average received SNR $\overline{\gamma}$ in dB. For TIFR case, γ_o is 0.1. The fading channel parameters can be found in Table 1. The reason behind this choice is to match those produced in [7]. The normalized average channel capacity curves for the ORA scheme precisely match those curves produced in [7], which provides a benchmark for the rest of our analysis. As expected, the SS case achieves better performance than the DS one. This is because shadowing exists in two scattering regions around the Tx and Rx in the DS scenario. Whereas in the SS one, shadowing is present in only one of the two regions. Another method to validate this fact is by computing the amount of fading using (15) and (18) for the DS case and SS one respectively. $\mathcal{AF}_{DS} = 6.02$ and $\mathcal{AF}_{SS} = 3.32$. As we can see, the amount of fading is greater for the DS case than the SS one.

In addition, the OPRA method achieves the optimal channel capacity in comparison to other methods. As opposed to using the fixed average power to send a signal in ORA, the Tx in the OPRA case modifies its transmit power in accordance with the instantaneous channel status. At the high SNR region, the average channel capacity in ORA and OPRA strategies converges. This is because $\gamma_o \to 1$ as $\overline{\gamma} \to \infty$, which indicates

$$C_{\mathrm{E}}^{\mathrm{DS}} = \frac{-\mathbb{B}}{A} \log_2\left(\frac{\mathbb{S}_{DS}}{\Gamma(A)} G_{3,3}^{3,3}\left(\frac{m_1 m_2}{\overline{\gamma}} \middle| \begin{matrix} 1-\alpha_2, 1-\alpha_1, 1 \\ m_1, m_2, A \end{matrix}\right)\right) \tag{43}$$

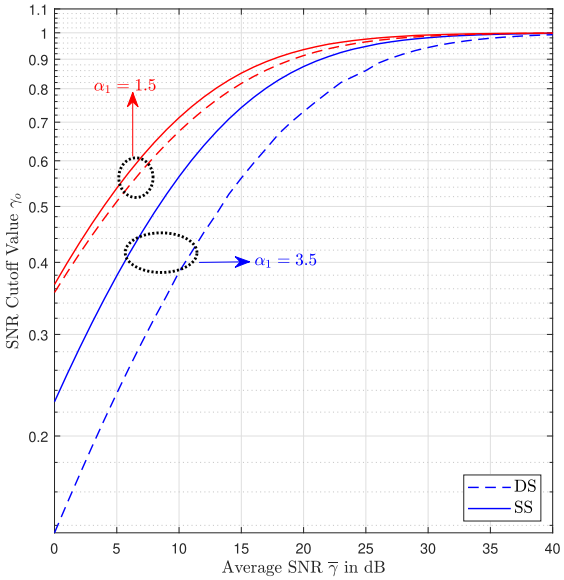

FIGURE 2. Optimal cutoff SNR, γ_o, versus the average SNR $\overline{\gamma}$ in dB.

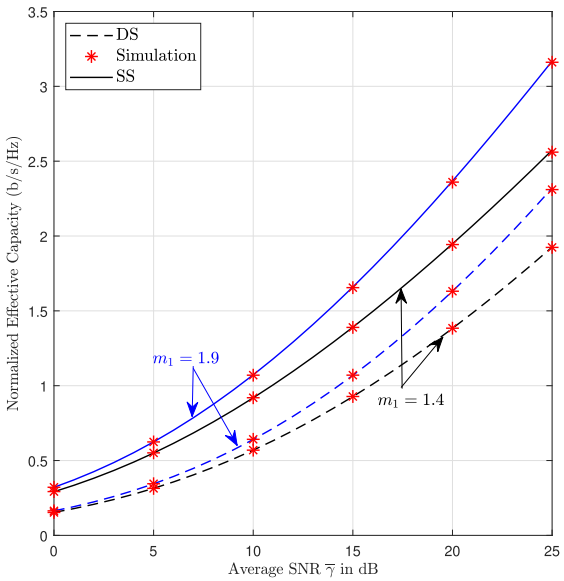

FIGURE 3. Normalized effective capacity versus average SNR in dB.

that the transmit power under the OPRA case becomes almost equal to the average power. The corresponding optimum cut-off values can be found in Fig. 2.

Fig. 2 provides the optimal cut-off SNR values, γ_o, for OPRA as a function of the average SNR $\overline{\gamma}$ in dB. The channel parameters are the same as Fig. 1, while varying α_1 ($\alpha_2 = \alpha_1 + 0.1$). In order to produce this figure, (27) and (29) were evaluated numerically for the DS case, and SS one respectively. It is clear that γ_o increases as the average SNR increases, with a maximum value of 1. For the same value of average SNR, the cutoff value decreases as the channel goes through severe shadowing, which is indicated by increasing the value of α_1.

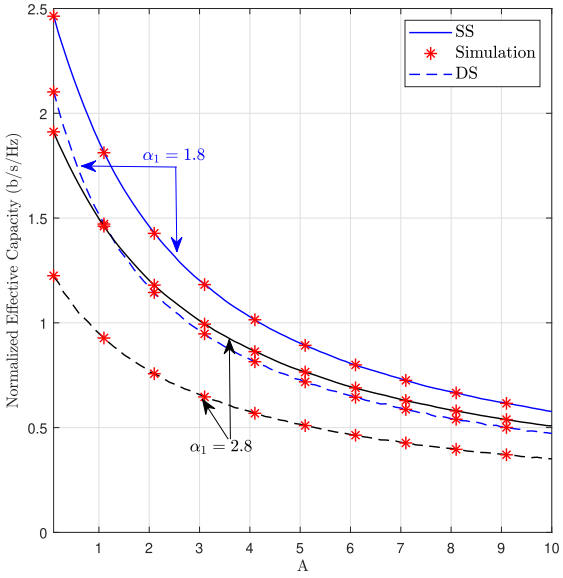

FIGURE 4. Normalized effective capacity versus *A*.

In Fig. 3, the normalized effective capacity, $C_E/\mathbb{B}$, is plotted as a function of the average received SNR $\overline{\gamma}$ in dB. The fading channel parameters were chosen to become ($m_2 = m_1 + 0.2, \alpha_1 = 3.1$, and $\alpha_2 = 3.3$) and $A = 3$. The curves produced through our analysis precisely match those produced via Monte Carlo simulation, which in turn validates our analysis. As the value of m_1 increases, it becomes evident that capacity improves because the multipath effect of the channel diminishes. As anticipated, the SS scenario outperforms the DS scenario in terms of effective capacity performance.

In Fig. 4, the normalized effective capacity, denoted as $C_E/\mathbb{B}$, is plotted versus the parameter A. The parameters characterizing the fading channel were deliberately set as follows: $m_1 = 1.5, m_2 = 1.8, \alpha_2 = \alpha_1 + 0.2$, and $\overline{\gamma} = 10$ dB. As the value of A increases, the effective capacity decreases. The normalized effective capacity decreases as the channel experiences significant shadowing. This is evident when the parameter α_1 increases.

VII. CONCLUSION

In this paper, closed-form expressions for the amount of fading as well as average ergodic channel capacity under different power adaptation schemes were evaluated. Based on the obtained results, the performance of OPRA significantly outperforms all other techniques. This superiority is primarily attributed to the substantial power allocation required by channel inversion to mitigate the effects of severe channel fading. But, it does come at the expense of complexity and the need for a feedback channel between Tx and Rx. Furthermore, closed-form equations for the effective capacity were formulated. These expressions are in terms of the Gamma function or Meijer *G*-function, both of them are built-in functions in MATLAB, which makes our expressions easy to implement. Then, all theoretical findings were verified through Monte Carlo simulations.

REFERENCES

[1] M. Mozaffari, W. Saad, M. Bennis, Y.-H. Nam, and M. Debbah, "A tutorial on UAVs for wireless networks: Applications, challenges, and open problems," *IEEE Commun. Surv. Tuts.*, vol. 21, no. 3, pp. 2334–2360, thirdquarter 2019.

[2] I. Bor-Yaliniz, M. Salem, G. Senerath, and H. Yanikomeroglu, "Is 5G ready for drones: A look into contemporary and prospective wireless networks from a standardization perspective," *IEEE Wireless Commun.*, vol. 26, no. 1, pp. 18–27, Feb. 2019.

[3] Y. Zeng, Q. Wu, and R. Zhang, "Accessing from the sky: A tutorial on UAV communications for 5G and beyond," *Proc. IEEE*, vol. 107, no. 12, pp. 2327–2375, Dec. 2019.

[4] D. Liu et al., "Opportunistic UAV utilization in wireless networks: Motivations, applications, and challenges," *IEEE Commun. Mag.*, vol. 58, no. 5, pp. 62–68, May 2020.

[5] B. Li, Z. Fei, and Y. Zhang, "UAV communications for 5G and beyond: Recent advances and future trends," *IEEE Internet Things J.*, vol. 6, no. 2, pp. 2241–2263, Apr. 2019.

[6] N. Parvaresh, M. Kulhandjian, H. Kulhandjian, C. D'Amours, and B. Kantarci, "A tutorial on AI-powered 3D deployment of drone base stations: State of the art, applications and challenges," *Veh. Commun*, vol. 36, 2022, Art. no. 100474.

[7] P. S. Bithas, V. Nikolaidis, A. G. Kanatas, and G. K. Karagiannidis, "UAV-to-ground communications: Channel modeling and UAV selection," *IEEE Trans. Commun.*, vol. 68, no. 8, pp. 5135–5144, Aug. 2020.

[8] P. S. Bithas, V. Nikolaidis, and A. G. Kanatas, "A new shadowed double-scattering model with application to UAV-to-ground communications," in *Proc. IEEE Wireless Commun. Netw. Conf.*, 2019, pp. 1–6.

[9] D. Dixit, N. Kumar, S. Sharma, V. Bhatia, S. Panic, and C. Stefanovic, "On the ASER performance of UAV-based communication systems for QAM schemes," *IEEE Commun. Lett.*, vol. 25, no. 6, pp. 1835–1838, Jun. 2021.

[10] R. Polus and C. D'Amours, "On the performance of MRC receivers in UAV-to-Ground channels with shadowing," *IEEE Wireless Commun. Lett.*, vol. 12, no. 7, pp. 1249–1253, Jul. 2023.

[11] M.-S. Alouini and A. J. Goldsmith, "Capacity of rayleigh fading channels under different adaptive transmission and diversity-combining techniques," *IEEE Trans. Veh. Technol.*, vol. 48, no. 4, pp. 1165–1181, Jul. 1999.

[12] A. J. Goldsmith and P. P. Varaiya, "Capacity of fading channels with channel side information," *IEEE Trans. Inf. Theory*, vol. 43, no. 6, pp. 1986–1992, Nov. 1997.

[13] M.-S. Alouini and A. Goldsmith, "Capacity of nakagami multipath fading channels," in *Proc. IEEE 47th Veh. Technol. Conf. Technol. Motion*, 1997, pp. 358–362.

[14] H. Zhao, Z. Liu, and M.-S. Alouini, "Different power adaption methods on fluctuating two-ray fading channels," *IEEE Wireless Commun. Lett.*, vol. 8, no. 2, pp. 592–595, Apr. 2019.

[15] H. Zhao, L. Yang, A. S. Salem, and M.-S. Alouini, "Ergodic capacity under power adaption over fisher–snedecor $\mathcal{F}$ fading channels," *IEEE Commun. Lett.*, vol. 23, no. 3, pp. 546–549, Mar. 2019.

[16] D. Wu and R. Negi, "Effective capacity: A wireless link model for support of quality of service," *IEEE Trans. Wireless Commun.*, vol. 2, no. 4, pp. 630–643, Jul. 2003.

[17] S. K. Yoo, S. L. Cotton, P. C. Sofotasios, S. Muhaidat, and G. K. Karagiannidis, "Effective capacity analysis over generalized composite fading channels," *IEEE Access*, vol. 8, pp. 123756–123764, 2020.

[18] M. Nakagami, "The m-distribution–A general formula of intensity distribution of rapid fading," in *Statistical Methods in Radio Wave Propagation*. New York, NY, USA: Elsevier, 1960, pp. 3–36.

[19] V. Witkovsky, "Computing the distribution of a linear combination of inverted gamma variables," *Kybernetika*, vol. 37, pp. 79–90, 2001.

[20] I. S. Gradshteyn and I. M. Ryzhik, *Table of Integrals, Series, and Products*. Cambridge, MA, USA: Academic Press, 2014.

[21] P. S. Chauhan, S. Kumar, A. Jain, and L. Hanzo, "An asymptotic framework for fox's H-fading channel with application to diversity-combining receivers," *IEEE Open J. Veh. Technol.*, vol. 4, pp. 404–416, 2023.

[22] M. K. Simon and M.-S. Alouini, *Digital Communication Over Fading Channels*. New York, NY, USA: Wiley, 2001.

[23] V. Adamchik and O. Marichev, "The algorithm for calculating integrals of hypergeometric type functions and its realization in REDUCE system," in *Proc. Int. Symp. Symbolic Algebr. Computation*, 1990, pp. 212–224.

[24] A. M. Mathai and R. K. Saxena, *Generalized Hypergeometric Functions With Applications in Statistics and Physical Sciences*, vol. 348. Berlin, Germany: Springer, 2006.

[25] Y. Abo Rahama, M. H. Ismail, and M. S. Hassan, "Capacity of fox's h-function fading channel with adaptive transmission," *Electron. Lett.*, vol. 52, no. 11, pp. 976–978, 2016.

REMON POLUS (Graduate Student Member, IEEE) received the B.Sc. and M.Sc. degrees in electrical engineering from Alexandria University, Alexandria, Egypt, in 2016 and 2021, respectively. He is currently working toward the Ph.D. degree with the School of Electrical Engineering and Computer Science, University of Ottawa, Ottawa, ON, Canada. From 2016 to 2021, he was a Teaching Assistant with the Department of Electrical Engineering, Alexandria University. His research interests include wireless communications, signal processing, and MIMO systems.

CLAUDE D'AMOURS (Member, IEEE) received the B.A.Sc., M.A.Sc., and Ph.D. degrees in electrical engineering from the University of Ottawa, Ottawa, ON, Canada, in 1990, 1992, and 1995, respectively. In 1992, he was a Systems Engineer with Calian Communications Ltd. In 1995, he joined the Communications Research Centre, Ottawa, as a Systems Engineer. In 1995, he joined the Department of Electrical and Computer Engineering, Royal Military College of Canada, Kingston, ON, Canada, as an Assistant Professor. He joined the School of Information Technology and Engineering (SITE), which has since been renamed as the School of Electrical Engineering and Computer Science (EECS), University of Ottawa, as an Assistant Professor, in 1999. From 2007 to 2011, he was the Vice Dean of Undergraduate Studies with the Faculty of Engineering, University of Ottawa, where he was the Director of the School of EECS, from 2013 to 2022. His research interests include physical layer technologies for wireless communications systems, notably in multiple access techniques, and interference cancellation.